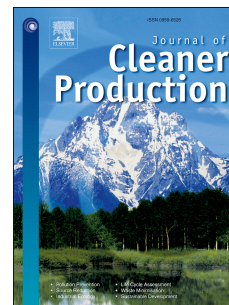


# Journal Pre-proof

Healing characterisations of waste-derived bitumen based on crack length:  
Laboratory and modelling

Linglin Li, Yang Yang, Yangming Gao, Yuqing Zhang



PII: S0959-6526(21)02484-7

DOI: <https://doi.org/10.1016/j.jclepro.2021.128269>

Reference: JCLP 128269

To appear in: *Journal of Cleaner Production*

Received Date: 10 June 2020

Revised Date: 19 June 2021

Accepted Date: 8 July 2021

Please cite this article as: Li L, Yang Y, Gao Y, Zhang Y, Healing characterisations of waste-derived bitumen based on crack length: Laboratory and modelling, *Journal of Cleaner Production* (2021), doi: <https://doi.org/10.1016/j.jclepro.2021.128269>.

This is a PDF file of an article that has undergone enhancements after acceptance, such as the addition of a cover page and metadata, and formatting for readability, but it is not yet the definitive version of record. This version will undergo additional copyediting, typesetting and review before it is published in its final form, but we are providing this version to give early visibility of the article. Please note that, during the production process, errors may be discovered which could affect the content, and all legal disclaimers that apply to the journal pertain.

© 2021 Published by Elsevier Ltd.

To: Journal of Cleaner Production

19 June 2021

### **Credit Author Statement**

**Re:** submission of paper (revised version) entitled “Healing Characterisations of Waste-derived Bitumen Based on Crack Length” by Linglin Li, Yang Yang, Yangming Gao, and Yuqing Zhang to Journal of Cleaner Production.

The authors confirm contribution to the paper as follows:

**Linglin Li:** Formal analysis, Funding acquisition, Investigation, Methodology, Validation, Writing - original draft.

**Yang Yang:** Investigation, Methodology, Resources.

**Yangming Gao:** Investigation, Methodology, Resources.

**Yuqing Zhang:** Funding acquisition, Methodology, Supervision, Writing - review & editing.

All authors interpreted and reviewed the results and approved the manuscript.

Sincerely yours,



Signed by Corresponding Author on behalf of all authors.

**Yuqing Zhang, PhD**

Senior Lecturer in Highway Engineering

Aston Institute of Materials Research (AIMR)

Engineering System & Management (ESM)

Aston University

Address: Aston Triangle, Birmingham, B4 7ET, U.K.

Tel: +44 121- 204- 3391

Email: y.zhang10@aston.ac.uk

## Healing Characterisations of Waste-derived Bitumen Based on Crack Length: Laboratory and Modelling

**Linglin Li**, Ph.D.

Associate Professor<sup>1</sup> & Marie Skłodowska-Curie Research Fellow<sup>2</sup>

<sup>1</sup>Automotive and Transportation Engineering College

Hefei University of Technology, Hefei, Anhui, China, 230009

<sup>2</sup>Aston Institute of Materials Research

Department of Civil Engineering

Aston University, MB226, Aston Triangle, Birmingham, B4 7ET, U.K.

Email: [l.li28@aston.ac.uk](mailto:l.li28@aston.ac.uk)

**Yang Yang**, Ph.D.

Lecturer in Department of Civil Engineering

Aston University, MB226E, Aston Triangle, Birmingham, B4 7ET, U.K.

Email: [y.zhang10@aston.ac.uk](mailto:y.zhang10@aston.ac.uk)

**Yangming Gao**, Ph.D.

Aston Institute of Materials Research

Department of Civil Engineering

Aston University, MB226, Aston Triangle, Birmingham, B4 7ET, U.K.

Email: [gaoy14@aston.ac.uk](mailto:gaoy14@aston.ac.uk)

**Yuqing Zhang**, Ph.D.

Senior Lecturer in Highway Engineering, Engineering Systems & Management Group (ESM)

Deputy Director, Aston Institute of Materials Research

Aston University, MB226E, Aston Triangle, Birmingham, B4 7ET, U.K.

Email: [y.zhang10@aston.ac.uk](mailto:y.zhang10@aston.ac.uk)

(Corresponding Author)

Word Count: 9872

Submitted [19/June/2021]



## 44 1. Introduction

45 Petroleum-derived bitumen, the residue from crude oil refining, is used as a binder in asphalt  
46 concrete for constructing and maintaining over 95% of the UK's transport infrastructures,  
47 such as roads (Lvel et al., 2020), highways (Li et al., 2015), airport runways (Li, Q. et al.,  
48 2018) and car parks (Azam et al., 2018). However, there has been increased concerns over  
49 the negative environmental effects (e.g., global greenhouse gas emissions) of the petroleum  
50 industry (Ali et al., 2019), which increases the demand for eco-friendly binders for pavement  
51 construction. Furthermore, petroleum-derived bitumen makes up about 5% of the road  
52 construction but accounts for approximately half of the cost of materials used to produce an  
53 asphalt mixture. Hence, there would be substantial benefits to the environment and economic  
54 cost if an eco-friendly and renewable bitumen is developed and implemented.

55 There are a couple of waste materials that have been effectively utilised in asphalt pavement,  
56 which substantially enhances engineering performances of asphalt mixture and reduces the  
57 environmental harm. Marble wastes are commonly used as fine aggregate and filler in asphalt  
58 mixture. Kofteci et al. (2018) evaluated the usability of marble waste in asphalt mixture.  
59 They reported that marble waste can effectively increase the Marshall stability and reduce the  
60 flow value of the asphalt mixture. In addition, they found that the involvement of marble  
61 waste promoted the indirect tensile strength and resistance to moisture damage and abrasion  
62 wear. Recycled paper mill sludge is also documented to partially substitute the mineral filler  
63 to improve the asphalt performance. Chew et al. (2020) investigated the mechanical  
64 properties of asphalt mixture modified by recycled paper (dry process) mill sludge from the  
65 microscopic perspective. They found that recycled paper mill sludge can effectively promote  
66 the mechanical properties (e.g., resilient modulus, Leutner shear and dynamic creep) of  
67 asphalt mixture. The fundamental reason of the above observations is that recycled paper mill  
68 sludge forms a type of lapped antenna, which promotes mechanical performance and binder-  
69 aggregate adhesion bonding of asphalt mixture. In addition to marble waste and paper sludge  
70 waste, solid waste of restaurant (de Azevedo et al., 2020) can also be utilised in asphalt  
71 mixture to enhance its performance. Jalkh et al. (2018) evaluated the impacts of oxidation on  
72 physicochemical and rheological performances of waste cooking oil and coffee grounds oil  
73 for potential use as rejuvenators of reclaimed bitumen from aged and damaged asphalt  
74 pavements. They concluded that the waste cooking oil and coffee grounds oil can be used as  
75 sustainable rejuvenators for reclaimed bitumen. In addition, the viscosity of the above oils  
76 can be customised by oxidation process (e.g., temperature and duration) to work well with the  
77 reclaimed bitumen.

78 Meantime, in the UK there are approximately 8 million tonnes of waste plastics and  
79 municipal solid waste (MSW) needed to be processed each year. Due to the difficulties in  
80 their logistics, sorting and reuse, almost all of them are landfilled, sea-dumping or  
81 incinerated. With the development of waste management techniques and implementation of a  
82 circular economy, people gradually find that one of the promising options to recycle most of  
83 these wastes is to convert them physically or chemically into durable construction materials  
84 for transport infrastructures (Abo El-Naga and Ragab, 2019; Romeo et al., 2018). Fethiza Ali  
85 et al. (2020) studied the effect of waste plastic on thermal-oxidative ageing of the bitumen.  
86 They found that waste plastic modified bitumen presented higher resistance to thermal-  
87 oxidative ageing (i.e., short-term ageing and long-term ageing) compared to the control  
88 bitumen. Tauste-Martínez et al. (2021) conducted an assessment of the effect of recycled  
89 low-density polyethylene (LDPE) on the long-term performance of the bitumen. The Atomic  
90 Force Microscopy (AFM) and Multiple Stress Creep and Recovery (MSCR) results proved  
91 that recycled LDPE can effectively improve the durability of the bitumen. Karmakar and

92 Kumar Roy (2021) investigated the influence of plastic waste on moisture damage of  
93 bituminous materials with the test methods of FTIR, AFM, modified Marshall immersion,  
94 and indirect tensile strength. The results indicated that plastic waste can be utilised as an  
95 effective moisture resistive modifier to fabricate a durable asphalt mix in the wearing course  
96 of asphalt pavement. Ramli et al. (2021) designed a modified asphalt mixture with waste  
97 plastic polypropylene to enhance its performance of horizontal deformation. The horizontal  
98 deformation measured from the test showed that waste plastic polypropylene strengthened the  
99 deformation properties of the mixture without any negative effect.

100 Regarding the MSW, more commonly known as trash or garbage, the main components are  
101 the product packaging, grass clippings, furniture, clothing, bottles, food scraps, newspapers,  
102 appliances, and paint, all of which comes from the residential homes, schools, hospitals, and  
103 businesses. In recent years, the possibility of recycling the above MSW in pavement  
104 engineering attracts increased attention and quickly leads to hot issues. Spreadbury et al.  
105 (2021) evaluated the field performances (i.e., resilient modulus and permanent deformation)  
106 of MSW incineration bottom ash as a base material of a road. They found that the resilient  
107 modulus and permanent deformation of this base layer were affected by the thickness,  
108 compaction effort, and moisture content of this layer. Based on these results, the authors  
109 proposed an optimal performance guideline regarding compact energy, thickness, and  
110 moisture control of the MSW incineration bottom ash. Yan et al. (2019) investigated  
111 properties (e.g., penetration, soft point, complex modulus, and creep stiffness) of asphalt  
112 mortar modified by MSW incineration fly ash. They concluded that: 1) MSW incineration fly  
113 ash slightly decreased the low-temperature performance of the mortar, and this negative  
114 effect could be ignored; 2) MSW incineration fly ash significantly enhanced the high-  
115 temperature properties of the mortar. Hence, compared with the traditional filler (e.g.,  
116 limestone mineral), MSW incineration fly ash could be a better option for asphalt fabrication  
117 and implementation due to its advantages of waste management, energy conservation, and  
118 performance enhancement.

119 Pyrolysis, which is a thermochemical decomposition of organic material that occurs at  
120 designed temperatures in the absence of oxygen, is employed as a method for waste disposal  
121 and energy recovery. There have been increasing research activities and industrial  
122 developments of pyrolysis of unrecycled waste plastics by using different types of reactors to  
123 produce pyrolysis bio-oil. Hariadi et al. (2021) quantified the effects of bio-oils pyrolysed  
124 from waste LDPE in three different reactor outlets. They found that the quality and quantity  
125 of the bio-oil were essentially affected by pyrolysis duration and temperature. The optimal  
126 pyrolysis temperature for the selected waste LDPE was 250 °C. Baena-González et al. (2020)  
127 reported the recovery of bitumen, olefinic solvents, aromatic compounds, and recycled  
128 polystyrene from pyrolysis oil from waste plastics. Their results showed that waste-derived  
129 bitumen (i.e., bitumen obtained from the pyrolysis oil) had a high potential to be a modifier  
130 for traditional petroleum bitumen by reducing its viscosity and soft point because the waste-  
131 derived bitumen contained 55.05 wt% of aromatics and 33.41 wt% of saturates. Moreover,  
132 due to its great application potential showed by the altered physical, chemical, mechanical  
133 and economical properties, pyrolysis oil derived from the MSW also has been regarded as a  
134 promising candidate to enhance the bitumen's engineering performance. Yang et al. (2018)  
135 presented an investigation on ageing and rheological properties of bio-oil from intermediate  
136 pyrolysis of the organic part of the MSW. They observed an obvious decrease in dynamic  
137 viscosity of the bio-oil after accelerated ageing, which was due to the decomposition of the  
138 semisolid organic agglomerates in the MSW during the intermediate pyrolysis. The reduced  
139 dynamic viscosity of the bio-oil (after ageing) indicated that it can be selected as a substitute  
140 for the light component in the petroleum bitumen for road construction and maintenance.

141 It is observed that the bitumen in the asphalt mixture, when exposed to cracking damage  
142 caused by thermal, vehicle and other loadings, can heal the cracks and restore partially or  
143 fully the original set of their physical, chemical, and mechanical properties. The healing can  
144 defer the initiation and evolution of the material deteriorations (e.g., fatigue crack) and  
145 eventually result in an extension of the service life of the asphalt pavement. A road  
146 performance prediction without accurately modelling the healing process in the bitumen will  
147 lead to a significant systematic error which could cause misleading conclusions or completely  
148 wrong decisions in material selections, road structural design or techno-economic analyses.  
149 Xu et al. (2021) employed three types of rejuvenators to quantify the healing effect on  
150 performance recoveries of the damaged bitumen. They found that the selected rejuvenators  
151 encapsulated in calcium alginate can effectively restore the physical, chemical, and  
152 rheological performances of the damaged bitumen. The fundamental reason for this  
153 phenomenon is that the released rejuvenator wets the cracks, diffuses into the damaged  
154 bitumen, and heals the bitumen eventually. Grossegger (2021) investigated the occurrence of  
155 an optimal healing time in the asphalt. He concluded that 1) healing potential was related to  
156 healing method, healing duration, and crack type; 2) optimal healing time only can be  
157 determined in a range due to the measurement uncertainty introduced by the heterogeneity of  
158 the asphalt. Chen et al. (2002) proposed a method for surface energy measurement of the  
159 asphalt, based on which they predicted the fatigue and healing performances of the asphalt.  
160 They concluded that healing performances of asphalt pavement were strongly correlated with  
161 the fundamental material properties such as relaxation modulus and advancing surface energy  
162 of the bitumen. The well-designed asphalt mixtures with the bitumen of better healing  
163 properties (e.g., modulus and surface energy) have been proved to provide better healing  
164 performance during the service life of the asphalt pavement. Thus, an increasing demand is  
165 substantially raised for a comprehensive understanding and accurate prediction of the healing  
166 performance of the bitumen, particularly for that novel bitumen modified by the waste  
167 plastics and MSW pyrolysis liquid, where their healing potential is completely unknown.

168 The healing of the bitumen is commonly quantified by the healing index, which is normally  
169 defined by a per cent ratio of the recovery of a material parameter after a rest interval to the  
170 one before the rest interval. The healing index was a highly empirical-based parameter  
171 because there were no agreed conclusions on which material parameter should be used in  
172 defining the healing index. It was regarded as an empirical indicator of the rate and capability  
173 at which healing proceeded (Little et al., 1999). Miglietta et al. (2021) assessed two types of  
174 healing index with the magnitude of stiffness and fatigue endurance gain, respectively. They  
175 emphasised the importance of considering the coupled effect between rest time and healing  
176 temperature to get a reliable evaluation of healing performance. Gallego et al. (2021)  
177 employed a thermomechanical method to evaluate the healing performance of the asphalt  
178 mixture. They defined the healing index by a ratio of initial indirect tensile strength of the  
179 undamaged asphalt to final indirect tensile strength of the healed asphalt, based on which the  
180 authors optimised the heat and re-compaction energy for the assisted healing of the asphalt.  
181 Yamaç et al. (2021) characterised the healing of asphalt mastic by the capsule containing  
182 waste oil, during which the healing index was defined by a ratio of maximum breaking load  
183 after the healing process to the one prior to the healing process. They concluded that the  
184 amount of capsule added into the asphalt and healing temperature were two critical factors  
185 affecting the healing performance of the asphalt. Li et al. (2020) proposed that the healing  
186 can be directly defined by crack length as the healing is a process of crack reduction,  
187 resulting in the recovery of the other material properties. They concluded that the crack  
188 length-based healing index was more fundamental and reliable to characterise healing  
189 properties of the bitumen, because it can eliminate the effects of nonlinear viscoelasticity,

190 frictional heat loss, and thixotropy.

191 This study aims to characterise the healing performance of two kinds of waste-derived  
 192 bitumen, including bio-oil modified bitumen using MSW pyrolysis liquid and plastic  
 193 modified bitumen by LDPE. The theoretical models of the healing of the bitumen based on  
 194 the DSR tests were firstly presented, followed by the DSR fatigue-healing tests and surface  
 195 energy experiments. This consisted of the fabrications of bio-oil modified bitumen and LDPE  
 196 modified bitumen, preparation of testing specimens, and cracking/healing and contact angle  
 197 tests of the virgin and PAV-aged waste-derived bitumen. Then, characterisations of the  
 198 healing performances of the virgin and PAV-aged control and waste-derived bitumen were  
 199 analysed in detail, based on which the effects of the bio-oil and waste plastics on the healing  
 200 rate and healing potential were quantified. The last section summarised the main  
 201 contributions of this paper.

## 202 **2. Theoretical Models for Healing of Bitumen**

### 203 **2.1 Healing Characterisation Based on Crack Length**

204 Dynamic shear rheometer (DSR) is commonly utilised to characterise viscoelastic properties  
 205 of the bitumen; additionally, it can be effectively used to evaluate and predict fatigue crack  
 206 performance of the bitumen by applying a rotational fatigue load. Zhang and Gao (2019)  
 207 proposed and successfully verified a damage mechanics-based crack growth model, which  
 208 was employed to calculate the crack length of the bitumen under a rotational shear fatigue  
 209 load based on the DSR test. The crack length in a strain-controlled DSR time sweep fatigue  
 210 test can be shown by **Equation (1)**:

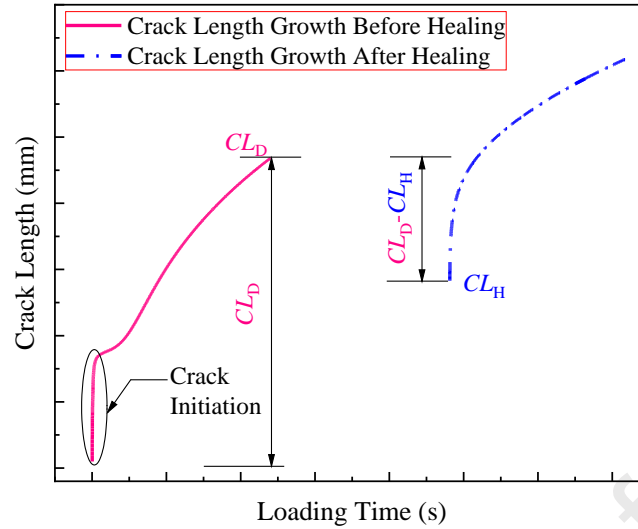
$$211 \quad CL = \left\{ 1 - \left[ \frac{|G_N^*| / \sin(\delta_N)}{|G_0^*| / \sin(\delta_0)} \right]^{1/4} \right\} r_0 \quad (1)$$

212 Where,  $CL$  is crack length of the bitumen at the  $N^{\text{th}}$  load cycle;  $|G_0^*|$  and  $\delta_0$  are dynamic shear  
 213 modulus and phase angle of the bitumen in the undamaged state, respectively;  $|G_N^*|$  and  $\delta_N$   
 214 are dynamic shear modulus and phase angle of the bitumen at the  $N^{\text{th}}$  load cycle in the  
 215 damaged state, respectively;  $r_0$  is original radius of the bitumen sample (i.e., 4mm in this  
 216 study).

217 Healing is a process of crack reduction; hence, it is reasonable to define the healing index  
 218 using the crack length, a justification of which can be found in the authors' previous paper  
 219 (Li et al., 2021). Based on **Equation (1)**, a new healing index defined in **Equation (2)** has  
 220 been successfully utilised to characterise the healing property of the bitumen (Li et al., 2020).  
 221 This newly defined parameter excludes the effects of viscoelasticity and thixotropy during the  
 222 rest period of rotational fatigue loads.

$$223 \quad \%HI = \frac{CL_D - CL_H}{CL_D} \times 100\% \quad (2)$$

224 Where,  $\%HI$  is healing index;  $CL_D$  is crack length at the last load cycle prior to the rest  
 225 duration;  $CL_H$  is crack length after the healing rest time. **Figure 1** shows an example of a  
 226 typical crack length before and after the healing time in a strain-controlled time sweep  
 227 fatigue-healing test.



228  
229 **Figure 1.** Crack length growth in a strain-controlled time sweep fatigue-healing test

230 Lytton (2000) proposed that healing of the bitumen depended on its surface energy ( $\Gamma_h$ )  
231 calculated from advancing contact angles, in which the non-polar component ( $\Gamma_h^{LW}$ ) sourced  
232 from Lifshitz-Van der Waals force and the polar component ( $\Gamma_h^{AB}$ ) resulted from Lewis acid-  
233 base force. There existed two healing mechanisms including short-term healing and long-  
234 term healing in its whole process. He noted that the short-term healing rate ( $\dot{h}_1$ ) depended  
235 primarily on  $1/\Gamma_h^{LW}$ , and the long-term healing rate ( $\dot{h}_2$ ) depended mainly on  $\Gamma_h^{AB}$ . Based on  
236 the above conclusions, Lytton proposed two useful models shown in **Equation (3)** to evaluate  
237  $\dot{h}_1$  and  $\dot{h}_2$ .

$$238 \quad \begin{cases} \dot{h}_1 = a_1 \left( \frac{1}{\Gamma_h^{LW} G_1} \right)^{b_1 m'} \\ -\log(\dot{h}_2) = a_2 \left[ -\log\left( \frac{\Gamma_h^{AB}}{G_1} \right) \right]^{b_2 m'} \end{cases} \quad (3)$$

239 Where,  $a_1$  and  $b_1$  are fitting parameters for the short-term healing rate  $\dot{h}_1$ ;  $a_2$  and  $b_2$  are fitting  
240 parameters for the long-term healing rate  $\dot{h}_2$ .

241 Many researchers (Cheng, D. et al., 2002; Luo and Lytton, 2016; Si et al., 2002) also noted  
242 that the two healing rates occur simultaneously, and the real healing mechanism is the result  
243 of their coactions. They furtherly recommended that actual healing rate  $d(HI)/dt$  could be  
244 expressed by the Ramberg-Osgood model (Ramberg and Osgood, 1943) shown in **Equation**  
245 **(4)**:

$$246 \quad \frac{d(HI)}{dt} = \dot{h}_2 + \frac{\dot{h}_1 - \dot{h}_2}{1 + \frac{\dot{h}_1 - \dot{h}_2}{h_\beta} (\Delta t)_h} \quad (4)$$

247 Where,  $(\Delta t)_h$  is the rest period between load applications; and  $h_\beta$  is the factor that varies  
248 between 0 and 1 and represents the healing potential, which is the maximum percentage of  
249 bitumen healing that can be achieved. The value of  $h_\beta$  is also empirically found to be related  
250 with  $\Gamma_h^{AB}/\Gamma_h^{LW}$ , and can be determined by **Equation (5)** (Luo, 2012):

$$h_{\beta} = \alpha_{\beta} \left( \frac{\Gamma_h^{AB}}{\Gamma_h^{LW} G_1^2} \right)^{b_{\beta} m'} \quad (5)$$

Where,  $\alpha_{\beta}$  and  $b_{\beta}$  are fitting parameters for the healing potential,  $h_{\beta}$ .

It should be noted that although the Ramberg-Osgood model was originally used to describe the nonlinear relationship between stress and strain in materials near their yield points, there is no constitutive interpretation herein, and it is believed that the Ramberg-Osgood model was simply used to characterise healing rate and healing potential of the selected bitumen.

## 2.2 Calculation of Surface Energy of Bitumen

Surface energy (more correctly, surface free energy) is one of the critical parameters affecting the healing performance of the bitumen as shown in **Equation (3)**. However, it is not feasible to directly measure the bitumen surface energy, and one proven method to estimate it is to measure contact angles between the bitumen and selected probe liquids with the sessile drop method and then calculate the surface energy. In this approach, the drops of a small number of probe liquids are deposited on the surface of the bitumen sample and the contact angles between the liquids and the bitumen surface are captured and measured, based on which the surface energy can be calculated using the Young-Dupre equation (van Oss, 2002):

$$(1 + \cos \theta) \Gamma_{liquid} = 2 \left[ \sqrt{\Gamma^{LW} \Gamma_{liquid}^{LW}} + \sqrt{\Gamma^+ \Gamma_{liquid}^-} + \sqrt{\Gamma^- \Gamma_{liquid}^+} \right] \quad (6)$$

Where,  $\theta$  is contact angle between the bitumen and the probe liquid drop;  $\Gamma_{liquid}$ ,  $\Gamma^{LW}$ ,  $\Gamma_{liquid}^{LW}$ ,  $\Gamma^+$ ,  $\Gamma^-$ ,  $\Gamma_{liquid}^+$ , and  $\Gamma_{liquid}^-$  are the surface energy of the probe liquid, the Lifshitz-van der Waals component of the bitumen, the Lifshitz-van der Waals component of the probe liquid, the Lewis acid component of the bitumen, the Lewis base component of the bitumen, the Lewis acid component of the probe liquid, and the Lewis base component of the probe liquid, respectively.

After obtaining the values of  $\Gamma^{LW}$ ,  $\Gamma^+$ , and  $\Gamma^-$ , the total surface energy  $\Gamma$  of a material can be calculated by:

$$\Gamma = \Gamma^{LW} + 2\sqrt{\Gamma^+ \Gamma^-} \quad (7)$$

## 3. Materials and Experimental Characterisation

### 3.1 Fabrication of Waste-derived Bitumen

Bitumen X70 was selected as a control and base bitumen to develop the waste-derived bitumen by mixing with waste materials (i.e., bio-oil or LDPE). Details of the production of the bio-oil can be found in the authors' previous publication (Yang et al., 2018). The concentrations of bio-oil and LDPE in the modified bitumen were 5wt. % and 6wt. %, respectively. The detailed characterisation of the control bitumen, bio-oil, and LDPE can be found in **Table 1**.

**Table 1.** Characterisations of X70, bio-oil, and LDPE

		Measure	Value
X70 <sup>a</sup>	Penetration @25°C	dmm	45-80
	Softening Point	°C	≥45

	Force Ductility @5°C	J/cm <sup>2</sup>	>3
	Flash Point (Cleveland)	°C	>250
	Fraas Breaking Point	°C	≤-12
bio-oil <sup>b</sup>	Water Content	wt. %	25.4
	Solid Content	wt. %	19.3
	Higher Heating Value	MJ/kg	28.0
	Density	g/cm <sup>3</sup>	0.972
LDPE <sup>c</sup>	Melting Point	°C	126
	Melting Heat	MJ/kg	0.141
	Density	g/cm <sup>3</sup>	0.934
	Thermal Degradation Point	°C	220

285 <sup>a</sup> Data provided by the supplier. <sup>b</sup> Data referenced from the author's previous work (Yang et al., 2018). <sup>c</sup> Data  
 286 obtained from DSC and density tests.

287 To fabricate 5wt. % bio-oil modified bitumen, bio-oil was firstly put into a clean beaker  
 288 followed by adding a well-calculated mass of hot control bitumen. Then, a high shear mixer  
 289 is used to mix them homogenously at a speed of 150RPM for 30min at 150°C under a  
 290 nitrogen atmosphere. Regarding the 6wt. % LDPE modified bitumen, hot control bitumen  
 291 was firstly put into another clean beaker followed by adding accurately calculated mass of the  
 292 LDPE. Then, the high shear mixer is utilised to blend the LDPE at a speed of 900RPM for  
 293 90min at 180°C under a nitrogen atmosphere. The blending speed and time were selected to  
 294 ensure the LDPE was completely melted and distributed within the hot bitumen.

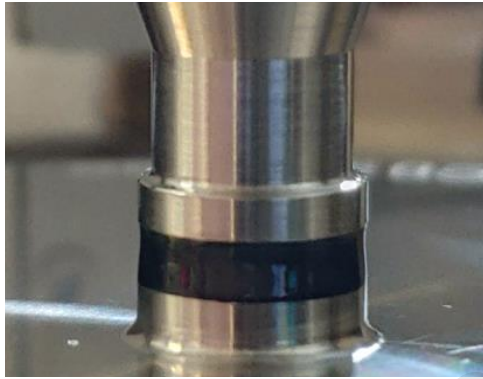
295 Then, part of three types of unaged bitumen (i.e., unaged control bitumen, newly fabricated  
 296 bio-oil modified bitumen and LDPE modified bitumen) were distributed into bitumen sample  
 297 bottle retainers to conduct the rolling thin-film oven (RTFO) ageing test at 163°C for 85min,  
 298 which is in consistent with the standard of AASHTO Designation T240-09 and ASTM  
 299 Designation D2872-04. RTFO ageing test provides simulated short-term aged bitumen for  
 300 engineering performance evaluations. The bitumen residue, from the RTFO ageing test, was  
 301 then placed in stainless steel pans and aged at 100°C for 20 hours in a vessel pressurised with  
 302 air to 2.10MPa (i.e., PAV ageing), which is in accordance with the standard of AASHTO  
 303 Designation R28-09. PAV ageing test provides simulated long-term (7 to 10 years) aged  
 304 bitumen for engineering performance evaluations, such as fatigue cracking and healing.

### 305 *3.2 Preparations of DSR and Surface Energy Test Specimens*

306 As mentioned in Section 2, the designed tests mainly include the DSR tests and surface  
 307 energy tests. The major goal of the DSR tests is to accurately measure the dynamic moduli  
 308 and phase angles of the undamaged, damaged, and healed bitumen. In terms of the surface  
 309 energy tests, the main objective is to obtain the advancing contact angles between the  
 310 bitumen and the probe liquids.

311 Before starting the tests, the bitumen samples stored in the containers were heated in the  
 312 laboratory oven at 165°C for 30min to reduce the material viscosity. Then hot bitumen was  
 313 carefully distributed into the silicon mould with a cavity of 4mm in diameter and 2 mm in  
 314 depth. After 15 minutes, the DSR sample was carefully demoulded from the mould and  
 315 installed and trimmed on the surfaces of the bottom and top plates to conduct the DSR tests  
 316 shown in **Figure 2**. The LAS, frequency sweep and healing tests were conducted on the DSR  
 317 using an 8 mm diameter parallel plate geometry and 2 mm gap setting, as shown in **Figure 2**.  
 318 To make the bitumen samples contact well with the DSR plates and reduce the heterogeneity  
 319 due to the fabrications of these samples, all bitumen samples were preheated to 80°C before

320 the tests started. After the DSR tests, both plates were checked carefully to make sure the  
 321 adhesions between them were still excellent. To examine the repeatability of the experiments,  
 322 three replicates were tested at each condition and additional replicates were added when the  
 323 repeatability COV of the target dynamic moduli and phase angles were greater than 5%, 10%,  
 324 and 5%, respectively, which is in consistent with the standard of EN 14770: 2012.

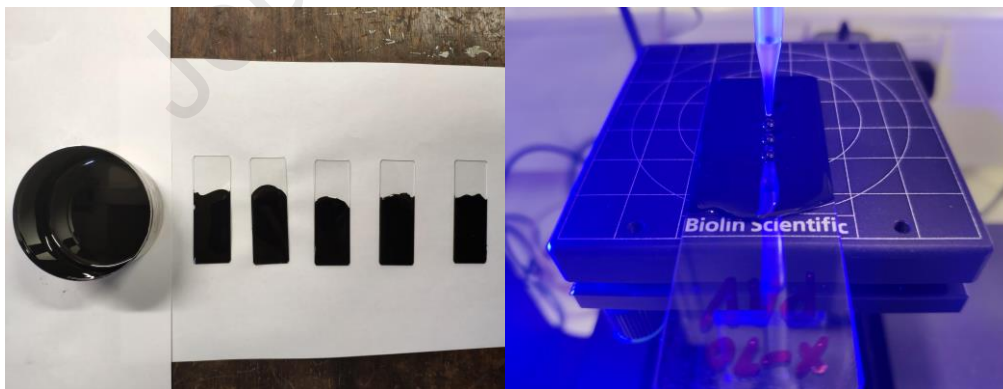


325

326 **Figure 2.** Trimmed configuration of an undamaged cylindrical bitumen sample

327 In this paper, surface energy for cracking and healing was measured by a versatile optical  
 328 tensiometer, where the Attension Theta Flex tensiometer was used. Microscope slides with  $76$   
 329  $\times 26 \times 1$ mm dimensions were cleaned with acetone and distilled water, and then dried by the  
 330 laboratory oven at  $60^{\circ}\text{C}$  for 30min. After that, the slides were dipped into the melted bitumen  
 331 for 10 seconds and then held out of the container for another 10 seconds to make the extra hot  
 332 bitumen drop off the slide. To get a flat and smooth surface of the bitumen sample, the above  
 333 process needs repeating at least 3 times, if necessary. Then the bitumen sample was cooled to  
 334 ambient temperature in a desiccator with anhydrous calcium sulphate crystals for 24 hours.

335 **Figure 3** presents the bitumen in the container and on the microscope slides, and the  
 336 installation of microscope slide coated with the bitumen on the Attension Theta Flex  
 337 tensiometer.



338

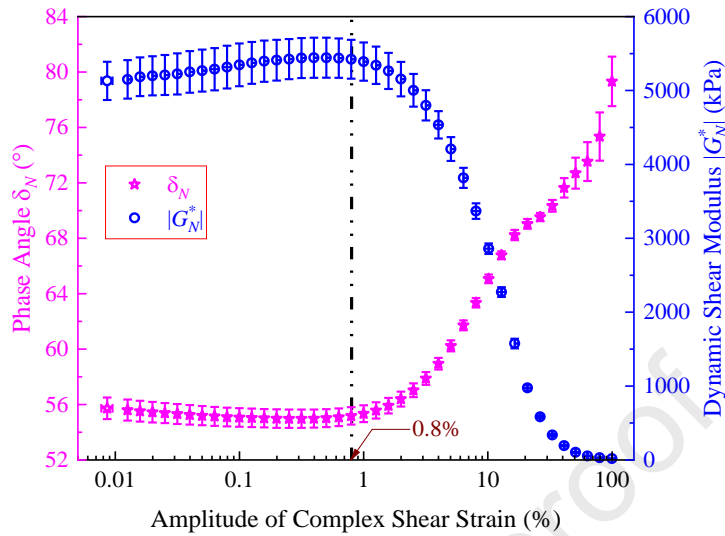
339 **Figure 3.** Bitumen in a container and on microscope slides, and contact angle test of the  
 340 bitumen by Attension Theta Flex tensiometer

### 341 **3.3 Experimental Characterisation of Bitumen**

#### 342 **a) Linear amplitude test to determine dynamic shear modulus and phase angle**

343 To calculate the crack length, healing index and other material parameters described in  
 344 Section 2, the dynamic shear modulus and phase angle of the undamaged bitumen need to be  
 345 calibrated firstly. **Figure 4** presents the dynamic shear moduli and phase angles from the

346 linear amplitude sweep (LAS) test of the unaged control bitumen conducted at 10Hz and  
 347 20°C. In this LAS test, the start and end complex shear strain levels were selected as 0.01%  
 348 and 100%, respectively.



349

350 **Figure 4.** Curves of shear modulus and phase angle versus shear strain from the LAS test  
 351 (10Hz and 20°C)

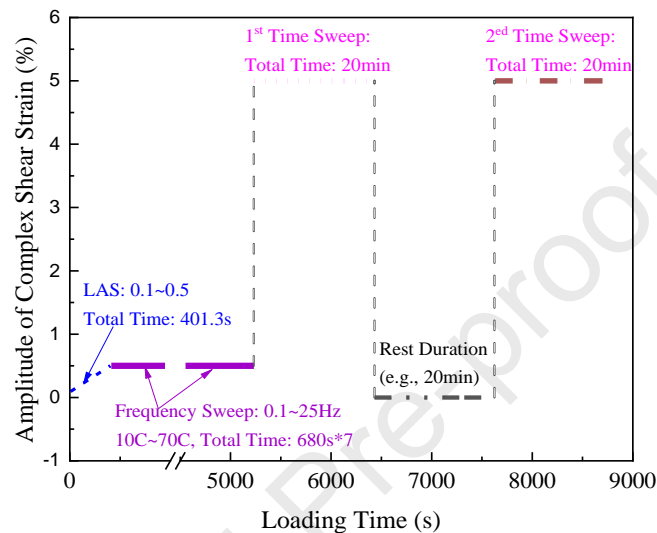
352 **Figure 4** shows that, in the LAS test, both dynamic shear modulus and phase angle vary little  
 353 or remain the same when the amplitude of the shear strain is low, e.g., less than 0.8%. This  
 354 implies that 0.8% is a critical threshold strain level, below which the unaged control bitumen  
 355 is undamaged at 10Hz and 20°C. When the amplitude of shear strain is over 0.8%, dynamic  
 356 shear modulus decreases and phase angle increases dramatically, which indicates that cracks  
 357 appear in the control bitumen. Theoretically, the  $|G^*_0|$  and  $\delta_0$  can be obtained by averaging the  
 358  $|G^*_N|$  and  $\delta_N$ , respectively, in a strain level between 0.01% and 0.8%, within which the  
 359 bitumen is in an undamaged condition. But practically, the sample-to-sample variation of the  
 360 bitumen needs to be considered, because the  $|G^*_0|$  and  $\delta_0$  measured herein will be used to  
 361 characterise the healing performance of the bitumen by integrating the following results of  
 362 frequency sweep tests and fatigue-healing tests. The DSR bitumen sample after the LAS tests  
 363 which is already damaged cannot be reused to investigate the healing property of the unaged  
 364 control bitumen. Therefore, a new DSR bitumen sample was employed to measure the  $|G^*_0|$   
 365 and  $\delta_0$  with the LAS start and end strain levels ranging from 0.1% and 0.5% (both less than  
 366 0.8%).  $|G^*_0|$  and  $\delta_0$  of the PAV-aged control bitumen, unaged and PAV-aged bio-oil modified  
 367 bitumen, and unaged and PAV-aged LDPE modified bitumen were obtained using the same  
 368 method.

### 369 **b) Frequency sweep tests and fatigue-healing tests to determine viscoelasticity and** 370 **healing properties**

371 Frequency sweep tests using the DSR were conducted at temperatures of 10°C, 20°C, 30°C,  
 372 40°C, 50°C, 60°C, and 70°C, and in a frequency range from 0.1Hz to 25Hz. The dynamic  
 373 shear moduli and phase angles were obtained at the above temperatures and frequencies, and  
 374 the master curves of the dynamic shear modulus and phase angle can be accurately  
 375 constructed (Li, L. et al., 2018a). Then, by using the interconversion equations for linear  
 376 viscoelastic material (Park and Schapery, 1999), shear relaxation modulus can be accurately  
 377 calculated, where the model parameter  $G_1$  and  $m'$  can be determined.

378 A fatigue-healing test was employed to characterise the fatigue-healing performance of the

379 bitumen. It consisted of a strain-controlled time sweep fatigue test (5%, 10Hz, 20°C) plus a  
 380 rest duration and followed by another strain-controlled time sweep fatigue test (5%, 10Hz,  
 381 20°C). The first part of the fatigue test was utilised to generate cracks in the bitumen and its  
 382 duration was 20 min. Different rest durations were used including 10s, 0.5min, 1min, 5min,  
 383 10min, and 20min (For the unaged control bitumen, 5s, 2min, and 40min were also used for  
 384 the rest durations). The second part of the fatigue test was used to obtain the cracking  
 385 performance after the healing rest was applied. The testing temperature was selected as 20°C.  
 386 The schematic plot of the loading sequences employed in the frequency sweep and the  
 387 fatigue-healing tests can be found in **Figure 5**.



388

389 **Figure 5.** Loading sequences of frequency sweep testing and fatigue-healing tests

### 390 c) Contact angle tests to determine surface energy of the bitumen

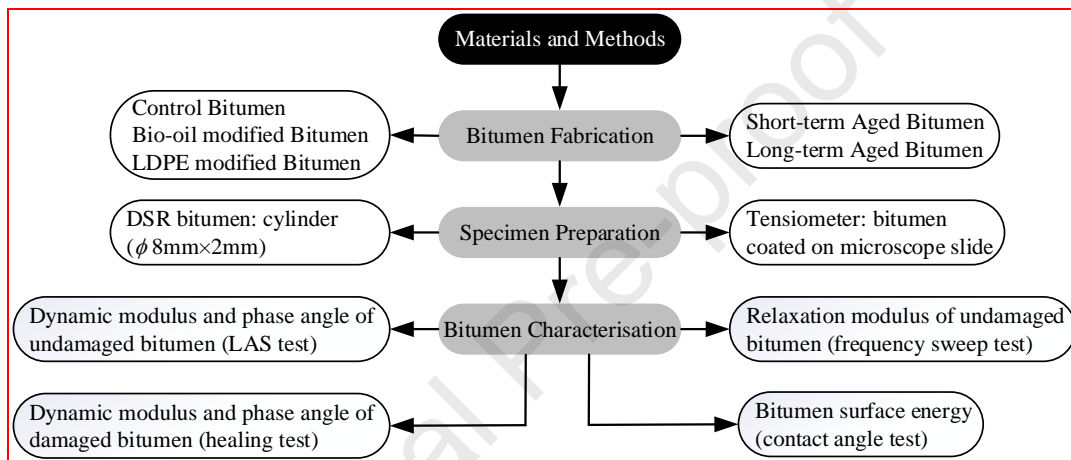
391 The sessile drop method (using Attension Theta Flex optical tensiometer) was adopted to  
 392 measure contact angles of bitumen surfaces with different probe liquids. The contact angle  
 393 results were then used to calculate surface energy components using **Equation (6)**. There are  
 394 two types of dynamic contact angles (i.e., advancing, and receding contact angles) that can be  
 395 measured by the mode of automatic dynamic contact angle built-in the tensiometer. Lytton et  
 396 al. (2005) stated that the surface energy calculated from the advancing contact angle  
 397 contributed to crack surface wetting and was related to the healing process; the receding  
 398 contact angle was associated with the de-wetting thus linked to the crack opening process.  
 399 For the healing purpose, this study used the advancing contact angles to determine the surface  
 400 energies of the materials.

401 Automatic dynamic contact angle experiments are conducted to obtain the advancing contact  
 402 angles between the bitumen samples and five preselected probe liquids (i.e., Ethylene glycol,  
 403 Water, Formamide, Glycerol, and Diiodomethane) with known surface energy components.  
 404 For each liquid, three clean and dry microscope slides coated with the bitumen were utilised  
 405 to reduce the variation of contact angle measurements. An automatic dispenser with a gauge  
 406 needle and an adapter containing different probe liquids was utilised herein. The adapter was  
 407 mounted to the dispenser and the needle was connected to the adapter. When the sample for  
 408 the experiment was in place of the tensiometer, key configurations of built-in software (i.e.,  
 409 OneAttension software) were set up immediately, including the creation of the user level,  
 410 selection of the experimental mode (i.e., automatic dynamic contact angle), completion of the  
 411 recipe (critical parameters of the experiment can be transmitted to the computer). Once all the  
 412 above controls have been set up, the experiment can be started and continued until its

413 completion.

414 There are two options (i.e., tilting cradle and thin needle method) available to obtain the  
 415 dynamic contact angles with the tensiometer. The tilting cradle method was used herein to  
 416 measure the advancing contact angles, which mainly includes the following steps: 1) A  
 417 droplet of the probe liquid is placed on the bitumen sample surface and tilting starts; 2) Once  
 418 the droplet starts moving on the bitumen sample surface, the advancing contact angle has  
 419 been reached, and the roll-off angle of the surface is also detected; 3) After setting the  
 420 baseline to the bitumen surface, contact angles can be imaged directly by the image recording  
 421 system of the tensiometer. The built-in software of the test equipment automatically  
 422 recognises and calculates the contact angles between the selected probe liquid and the  
 423 bitumen.

424 **Figure 6** summarises the experimental methodology employed in this section.



425

426

**Figure 6.** Flow chart of experimental methodology on healing characterisation

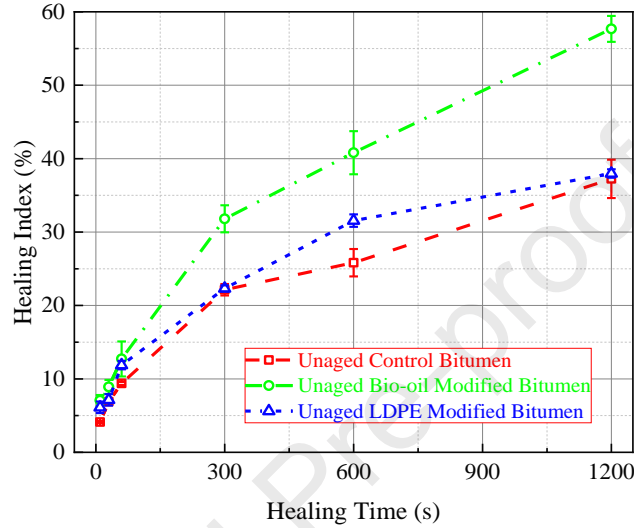
## 427 4. Results and Discussion

### 428 4.1 Enhancements of Healing Performances of Unaged Bitumen Modified by Bio- 429 oil or LDPE

430 **Figure 7** shows that healing indices of all three unaged bitumen increase with healing time,  
 431 which is consistent with the Ramberg-Osgood model shown in **Equation (4)**. Both the bio-oil  
 432 and LDPE can strengthen the healing performance of the unaged bitumen. Compared with the  
 433 LDPE, the enhancements due to the inclusion of bio-oil to the healing rate and healing  
 434 potential are more pronounced. The fundamental mechanism for this observation can be  
 435 explained that, compared to the bitumen molecules, the bio-oil is a kind of less viscous fluid  
 436 pyrolysed from municipal solid waste which can effectively soften the bitumen. Hence,  
 437 compared with the unaged control bitumen, the molecules of the bio-oil modified bitumen are  
 438 more diffusible, thus the cracks in the bio-oil modified bitumen are more healable. The above  
 439 explanation is well consistent with the results obtained by Sun and Zhou (2018).

440 The LDPE slightly enhances, not weakens, the healing performance of the unaged control  
 441 bitumen, which has been verified by the authors' previous paper (Li et al., 2021) using the  
 442 fundamental properties (e.g., surface energy) of the material to predict its healing  
 443 performance. This may be due to the diffusion of those short polymer chains in the LDPE to  
 444 the bitumen molecules to stimulate the healing of the material. Previous studies (Ahmedzade  
 445 et al., 2013; Farahani et al., 2017) show that the LDPE modified bitumen undergoes no

446 observable changes in functional groups relative to the control bitumen, which confirms that  
 447 this kind of modification of the control bitumen with LDPE is overwhelmed by physical  
 448 process. The short chains of the LDPE melted in the unaged bitumen tends to aggregate and  
 449 form a kind of network structure within a continuous polymer phase, which will potentially  
 450 increase the healing performance of the unaged bitumen. Therefore, the new formation of the  
 451 micro-network structure physically contributed by the melted LDPE is expected to be the  
 452 critical reason that slightly increase the healing performance of the unaged bitumen. More  
 453 details of fundamental understanding of LDPE's enhancements on bitumen healing will be  
 454 presented in the last part of this section.



455

456 **Figure 7.** Healing curves (healing index versus healing time) of the control bitumen, bio-oil  
 457 modified bitumen, and LDPE modified bitumen in unaged condition

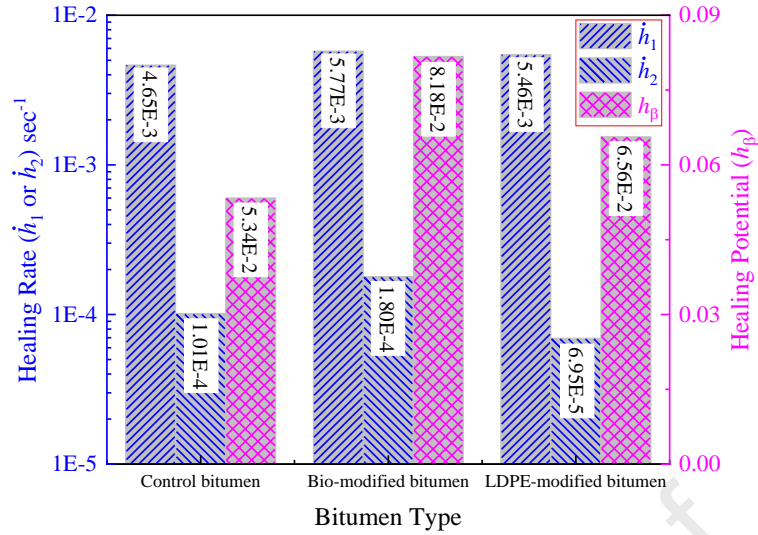
458 To further quantify the enhancements of the bio-oil and the LDPE to the healing performance  
 459 of the unaged bitumen, healing speed and healing potential models shown in **Equations**  
 460 **(3)~(5)** are determined and interpreted in detail.

461 According to the Ramberg-Osgood model shown in **Equation (4)**, the healing index can  
 462 alternatively be expressed by **Equation (8)**:

$$463 \quad HI = \dot{h}_2 (\Delta t)_h + h_\beta \ln \left[ 1 + \frac{\dot{h}_1 - \dot{h}_2}{h_\beta} (\Delta t)_h \right] \quad (8)$$

464 Substituting the measured healing index shown in **Figure 7**,  $\dot{h}_1$ ,  $\dot{h}_2$ , and  $h_\beta$  can be back-  
 465 calculated and presented in **Figure 8**.

466 **Figure 8** shows the results of the short-term healing rate, long-term healing rate and healing  
 467 potential of the three kinds of unaged bitumen. It is found that the long-term healing rate is  
 468 substantially smaller than the short-term healing rate, which means healing occurs mainly in a  
 469 short term. This observation is consistent with the one found in the existing research (Cheng,  
 470 D. et al., 2002). The short-term healing rate and healing potential dominate most of the  
 471 healing behaviours of the unaged bitumen. **Figure 8** also indicates that the unaged bio-oil  
 472 modified bitumen heals the most (having the highest  $h_\beta$  of the three), followed by the unaged  
 473 LDPE modified bitumen, and the unaged control bitumen heals the least. Both the bio-oil and  
 474 LDPE can increase the short-term healing rate of the unaged bitumen, and the unaged bio-oil  
 475 modified bitumen heals faster than the unaged LDPE modified bitumen in a short term.



476

477 **Figure 8.** Short-term healing rate ( $\dot{h}_1$ ), long-term healing rate ( $\dot{h}_2$ ) and healing potential ( $h_\beta$ )  
 478 of different kinds of unaged bitumen

479 The short-term healing rate, long-term healing rate and healing potential can also be predicted  
 480 using **Equation (3)** and **Equation (5)**. The parameters of  $m'$ ,  $G_1$  shown in these models are  
 481 presented in **Table 2**, which are calculated from the testing results of the frequency sweep  
 482 test (10Hz, 10~70°C) and LAS test (0.1%~0.5%, 20°C) of the unaged bitumen. The  
 483 calculation steps of determining  $m'$  and  $G_1$  are as follows: 1) Construction of the master curve  
 484 of shear dynamic modulus and phase angle of the unaged bitumen at the reference  
 485 temperature of 20°C by the time-temperature superposition principle (e.g., WLF equation); 2)  
 486 Calculation of Prony model parameters of shear relaxation modulus by the collocation  
 487 method (Park and Schapery, 1999) and the least squared regression minimization (Li, L. et  
 488 al., 2018b); 3) Interconversion between Prony model parameters and power model  
 489 parameters of shear relaxation modulus (i.e.,  $G(t) = G_1 t^{-m'}$ ).

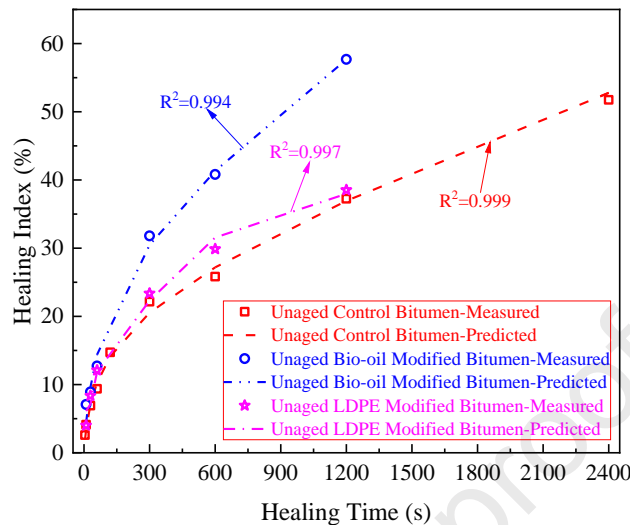
490 **Table 2.** Slope of double logarithmic relaxation modulus curve  $m'$ , initial shear relaxation  
 491 modulus  $G_1$ , Non-polar component  $\Gamma_h^{LW}$ , polar component  $\Gamma_h^{AB}$ , and total  $\Gamma_h$  advancing  
 492 surface energies of the unaged bitumen

	$m'$	$G_1$ (kPa)	$\Gamma_h$ (mJ/m <sup>2</sup> )	$\Gamma_h^{LW}$ (mJ/m <sup>2</sup> )	$\Gamma_h^{AB}$ (mJ/m <sup>2</sup> )
Control bitumen	0.7978	2398.8	14.36	13.95	0.41
Bio-modified bitumen	0.8290	480.2	12.50	12.39	0.11
LDPE-modified bitumen	0.7154	3680.2	27.16	27.09	0.07

493 The advancing contact angles between the unaged bitumen and the selected probe liquids are  
 494 measured by the tensiometer to calculate the advancing surface energy contributing to the  
 495 wetting and interdiffusion processes of the bitumen healing. **Table 2** also gives the  
 496 experimental results of the non-polar component, polar component, and total advancing  
 497 surface energies of the unaged bitumen.

498 Substituting the fundamental material constants ( $m'$ ,  $G_1$  and  $\Gamma_h$ ) to **Equations (3)** and **(5)**,  
 499 constants of  $a_i$  and  $b_i$  ( $i=1, 2$ , and  $\beta$ ) can be calculated with the aid of the Solver function in  
 500 Microsoft Excel. More importantly, with all the material constants known, **Equations (3)~(5)**  
 501 can be utilised to predict the healing index. **Figure 9** shows the measured and predicted  
 502 healing indices of the three bitumen samples in the unaged condition. It can be found that

503 **Equations (3)~(5)** can be effectively used to predict the healing index of the unaged bitumen.  
 504 This means, the healing curve of bitumen can be efficiently obtained once the material  
 505 properties (including relaxation modulus and surface energy) are known, which can  
 506 substantially reduce the experimental effort of the healing tests for the bitumen.

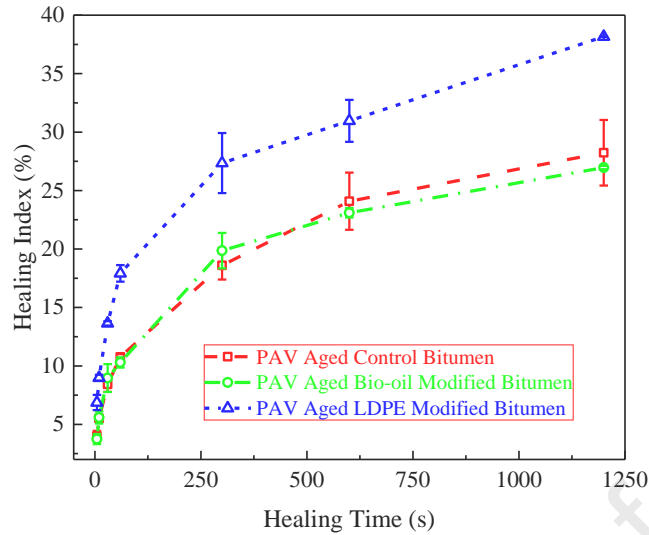


507

508 **Figure 9.** Comparisons between the predicted healing index using material properties  
 509 (relaxation modulus and surface energy) and the measured results from healing tests for  
 510 different bitumen materials in unaged condition.

#### 511 **4.2 Characterisations of Healing Performances of PAV-aged Control Bitumen, Bio-** 512 **oil Modified Bitumen, and LDPE Modified Bitumen**

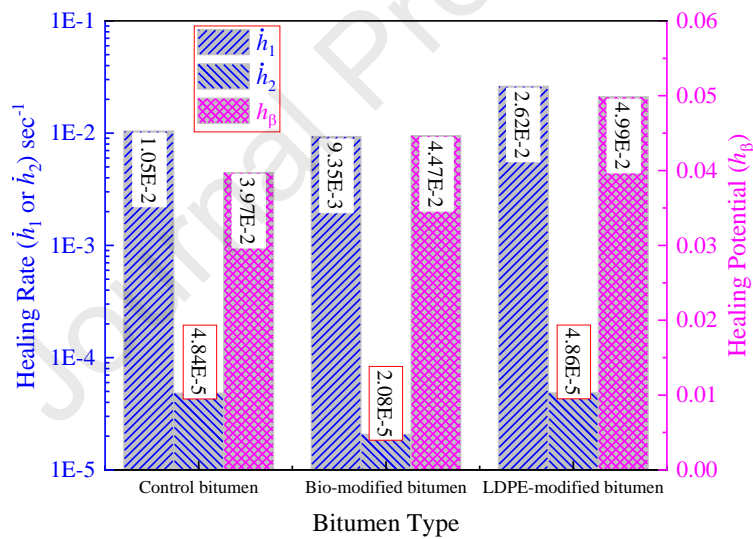
513 **Figure 10** shows that healing indices of the PAV-aged bitumen increase with the healing  
 514 time, which agrees well with the Ramberg-Osgood model shown in **Equation (4)**. The PAV-  
 515 aged bio-oil modified bitumen does not show better healing performance than that of the  
 516 PAV-aged control bitumen, the reason of which is that most of the bio-oil has evaporated  
 517 during the ageing process. Additionally, **Figures 7** and **10** show that the ageing process  
 518 substantially reduces the healing performances of the bio-oil modified bitumen and control  
 519 bitumen. The LDPE productively enhances the healing performance of the PAV-aged  
 520 bitumen, one of the key reasons of which is that the LDPE substantially reduces the ageing  
 521 rate of the bitumen (Nouali et al., 2020). Compared with the unaged LDPE modified bitumen,  
 522 it is worthy to notice that the ageing process does not effectively reduce the healing ability of  
 523 the LDPE modified bitumen. This observation can be interpreted as follows: 1) the molecular  
 524 chain of the LDPE in the control bitumen is very stable, and the ageing process does not  
 525 effectively decrease its activity and polarity (Nouali et al., 2020); 2) the PAV-aged control  
 526 bitumen itself has a relatively low healing ability, which implies that any changes to its  
 527 microstructure can potentially enhance its healing capability; and 3) the dispersed LDPE  
 528 molecular chain (observed by SEM in a previous study (García-Morales et al., 2004)) can be  
 529 swollen by the bitumen light components (i.e., saturate and aromatic), and the deformed  
 530 LDPE molecular chains due to rotational shear loads will recover their original shape during  
 531 the healing time. This significantly increases the motions of the light components of the  
 532 PAV-aged bitumen and then enhances the healing performance of the PAV-aged bitumen.  
 533 More details of the fundamental understanding of LDPE's enhancements on bitumen healing  
 534 will be presented in the last part of this section.



535

536 **Figure 10.** Healing curves of PAV-aged control bitumen, bio-oil modified bitumen, and  
 537 LDPE modified bitumen

538 Substituting the measured healing indices shown in **Figure 10** into **Equation (8)**, the short-  
 539 term healing rate  $\dot{h}_1$ , long-term healing rate  $\dot{h}_2$ , and healing potential  $h_\beta$  can be back-  
 540 calculated and the results are presented in **Figure 11**.



541

542 **Figure 11.** Short-term healing rate ( $\dot{h}_1$ ), long-term healing rate ( $\dot{h}_2$ ) and healing potential  
 543 ( $h_\beta$ ) of the PAV-aged bitumen

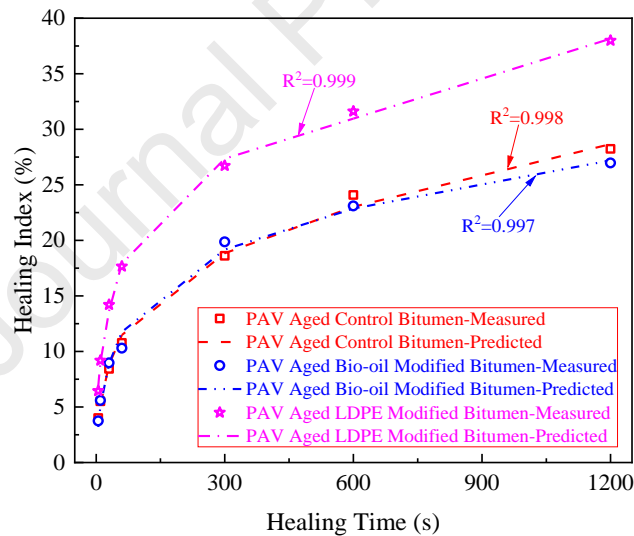
544 **Figure 11** shows that the long-term healing rate is significantly smaller than the short-term  
 545 healing rate, which indicates healing occurs mainly in a short term. The short-term healing  
 546 rate and healing potential dominate the healing behaviours of the PAV-aged bitumen. Since  
 547 most of the bio-oil has evaporated during the ageing process, differences in the short-term  
 548 healing rate and healing potential between the aged control bitumen and the aged bio-oil  
 549 modified bitumen can be neglected. **Figure 11** also shows that the PAV-aged LDPE modified  
 550 bitumen heals the most (having the highest  $h_\beta$ ), followed by the PAV-aged bio-oil bitumen  
 551 and control bitumen. The PAV-aged LDPE modified bitumen heals faster (having the highest  
 552  $\dot{h}_1$ ) than the PAV-aged control bitumen and the PAV-aged bio-oil modified bitumen.

553 As done in Section 4.1, healing speed and healing potential models shown in **Equations**  
 554 **(3)~(5)** are reutilised to verify the healing performances shown in **Figure 10**. **Table 3**  
 555 presents the values of  $m'$ ,  $G_1$ ,  $\Gamma_h^{LW}$ ,  $\Gamma_h^{AB}$ , and  $\Gamma_h$  of the control bitumen, bio-oil modified  
 556 bitumen, and LDPE modified bitumen after the PAV ageing.

557 **Table 3.** Slope of double logarithmic relaxation modulus curve  $m'$ , initial shear relaxation  
 558 modulus  $G_1$ , Non-polar component  $\Gamma_h^{LW}$ , polar component  $\Gamma_h^{AB}$ , and total  $\Gamma_h$  advancing  
 559 surface energies of the PAV-aged bitumen

	$m'$	$G_1$ (kPa)	$\Gamma_h$ (mJ/m <sup>2</sup> )	$\Gamma_h^{LW}$ (mJ/m <sup>2</sup> )	$\Gamma_h^{AB}$ (mJ/m <sup>2</sup> )
Control bitumen	0.7064	12251.3	17.62	17.25	0.36
Bio-modified bitumen	0.6598	12198.3	17.58	17.50	0.08
LDPE-modified bitumen	0.6399	21656.6	37.16	37.10	0.06

560 Substituting the fundamental material constants mentioned above to **Equations (3)** and **(5)**,  
 561 fitting constants of  $a_i$  and  $b_i$  ( $i=1, 2$ , and  $\beta$ ) can be back-calculated with the aid of the Solver  
 562 function in Microsoft Excel. After that, the healing index of the PAV-aged bitumen can be  
 563 predicted by **Equations (3)~(5)**. **Figure 12** presents the measured and predicted healing  
 564 indices of the PAV-aged bitumen. It can be concluded that **Equations (3)~(5)** can be  
 565 effectively used to predict the healing index of the PAV-aged bitumen once the material  
 566 properties (e.g., relaxation modulus and surface energy) are measured, which are expected to  
 567 substantially reduce the experimental effort of the healing tests of the PAV-aged bitumen.



568

569 **Figure 12.** Comparisons between the predicted healing index using material properties  
 570 (relaxation modulus and surface energy by **Equations (3)~(5)**) and the measured ones using  
 571 healing tests for different PAV-aged bitumen materials

### 572 **4.3 Fundamental Understanding of LDPE's Enhancements on Healing** 573 **Performance of Bitumen**

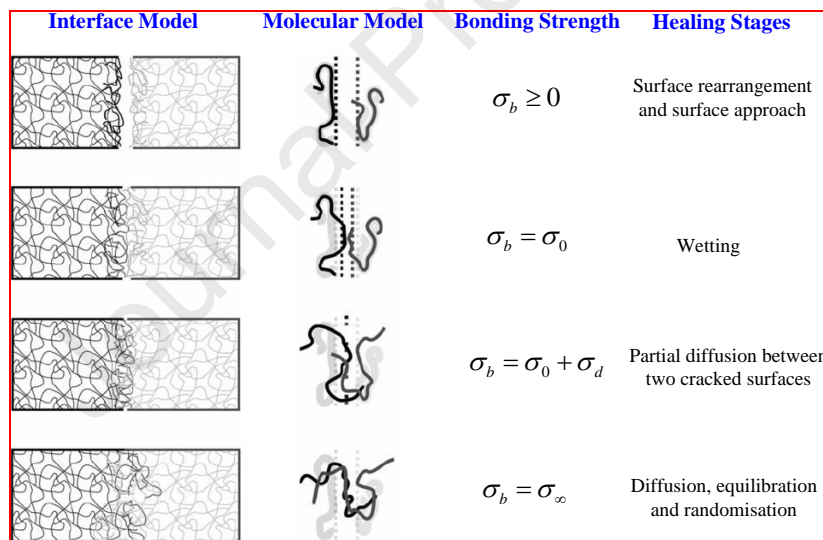
574 This section aims to provide a theoretical explanation of the LDPE's enhancements on  
 575 bitumen's healing performance. **Figure 13** shows the healing process of cracked surfaces in a  
 576 bitumen sample, which includes four steps, namely, surface rearrangement and approach,  
 577 wetting, diffusion, and randomisation. Note the four healing steps exist simultaneously for  
 578 the molecular chains of the bitumen (Bommavaram et al., 2009; Little et al., 2015). A well-

579 known theory of polymer healing was first ingeniously delivered by Wool and O'Connor  
 580 (Wool and O'Connor, 1981). They employed two functions (i.e., wetting distribution function  
 581  $\varphi(t)$  and intrinsic healing function  $R_h(t)$ ) to obtain the healing index %HI (originally called  
 582 recovery ratio) of mechanical properties of the polymer.

$$583 \quad HI\%(t) = \int_{-\infty}^t R_h(t-\tau) \frac{\partial \varphi(\tau)}{\partial \tau} d\tau \quad (9)$$

584 Where,  $t$  is present time;  $\tau$  is time history at which wetting distribution function and intrinsic  
 585 healing function are obtained. The polymer healing theories shown in **Equation (9)** are  
 586 demonstrated to be applicable for modelling bitumen healing as bituminous components and  
 587 behaviours are comparable to a complex polymer (Bhasin et al., 2011).

588 Crack wetting of the bitumen depicts the contact and cohesion of two approached crack  
 589 surfaces driven by the surface energy and bonding strength, leading to a definition of healing  
 590 potential. Hence, the crack wetting happens at the interfaces, briefly depicted as wetting  
 591 nucleation pools (Wool and O'Connor, 1981), of the cracked surfaces without inclusions of  
 592 bitumen chains' interdiffusion. Intrinsic healing of the bitumen describes the rate at which a  
 593 wetted crack interface recovers the mechanical performance of the intact material, leading to  
 594 a healing rate driven by Brownian motions of the bitumen molecules. The intrinsic healing  
 595 develops on account of the motions of bitumen chains, which are significantly affected by the  
 596 interdiffusions of neighbouring chains of the bitumen.



597

598 **Figure 13.** Schematic diagram of bitumen healing processes ( $\sigma_b$  is the bonding stress which  
 599 derives the healing of the cracked surfaces;  $\sigma_0$  is the recovered bonding strength due to  
 600 wetting;  $\sigma_d$  is the recovered bonding strength due to interdiffusions of material chains  
 601 between two cracked surfaces; and  $\sigma_\infty$  is the original bonding strength of the intact bitumen)

602 The LDPE modified bitumen shows better deformation recovery property than the control  
 603 bitumen because 1) the inclusion of LDPE makes the bitumen much stiffer than the control  
 604 one, as indicated by the increased modulus ( $G_1$ ) in **Table 2** for the unaged bitumen and **Table**  
 605 **4** for the aged bitumen; 2) the elongated LDPE molecular chains in the bitumen recovers to  
 606 their original shape when the external load is removed, which enhances the ability of the  
 607 bitumen to restore to its original state (García-Morales et al., 2004); and 3) the surface  
 608 energies (**Tables 2** and **3**) of the LDPE modified bitumen under unaged and aged conditions  
 609 are higher than those of the control bitumen. Because of the increased deformation recovery

610 and elevated surface energy, the LDPE modified bitumen has a reduced time to complete the  
 611 surface rearrangement, approach and wetting in the healing processes. This means the LDPE  
 612 in bitumen can accelerate the crack wetting process, thus leads to a higher wetting rate (i.e.,  
 613 the time derivative of the wetting distribution function  $\varphi(t)$  is higher) and eventually results in  
 614 higher healing. This is demonstrated by the higher short-term healing rate of the LDPE  
 615 modified bitumen than that of the control bitumen. For instance, **Figure 8** shows that the  
 616 short-term healing rate increased from  $4.65 \times 10^{-3} \text{sec}^{-1}$  to  $5.46 \times 10^{-3} \text{sec}^{-1}$  for the unaged  
 617 bitumen, and **Figure 11** shows that it increased from  $1.05 \times 10^{-3} \text{sec}^{-1}$  to  $2.62 \times 10^{-3} \text{sec}^{-1}$  for the  
 618 aged bitumen.

619 However, the LDPE in bitumen cannot accelerate the diffusion process to lead to faster  
 620 healing, as demonstrated by the much less changed long-term healing rate in **Figure 11**  
 621 between LDPE modified bitumen ( $4.86 \times 10^{-3} \text{sec}^{-1}$ ) and the control bitumen ( $4.84 \times 10^{-3} \text{sec}^{-1}$ ).  
 622 The fundamental reason is that the main diffusible components in bitumen to lead healing are  
 623 the light parts (i.e., saturate and aromatics). Some existing works of literature can support this  
 624 explanation, such as the one completed by Yang et al. (2020). Based on the dynamic shear  
 625 rheometer, they measured the data of complex viscosity and flow activation energy and found  
 626 that saturates and aromatics diffused much better than resins and asphaltenes in the bitumen.  
 627 The LDPE's molecular chains are much longer and heavier in molecular weight than those  
 628 light bitumen components. This makes the LDPE almost non-diffusible and contributes little  
 629 to long-term healing. In other words, the intrinsic healing function  $R_h(t)$  remains unchanged  
 630 between the LDPE modified bitumen and the control bitumen. Thus, the healing cannot be  
 631 enhanced by the LDPE by the improved molecular diffusion to increase the intrinsic healing.

632 In sum, the increased deformation recovery ability induced by LDPE in bitumen improves the  
 633 wetting rate of the cracked surfaces and leads to a higher short-term healing rate and bigger  
 634 healing. However, the LDPE in bitumen cannot accelerate the molecular diffusion to increase  
 635 the intrinsic healing or the long-term healing rate.

## 636 5. Summary and Conclusions

637 This paper characterised the healing performances of the unaged and PAV-aged waste-  
 638 derived bitumen (i.e., bio-oil modified bitumen, and LDPE modified bitumen) based on crack  
 639 length. The designed fatigue-healing test consisted of a strain-controlled time sweep fatigue  
 640 test plus a rest duration and followed by another strain-controlled time sweep fatigue test.  
 641 Crack length-based healing index and Ramberg-Osgood model were effectively utilised to  
 642 characterise the healing rate and healing potential of the unaged and PAV-aged bitumen. The  
 643 main findings and conclusions of this paper are summarized as follows:

- 644 (1) Both the bio-oil and LDPE can strengthen the healing performance of the unaged  
 645 bitumen. The unaged bio-oil modified bitumen heals the most (having the highest healing  
 646 potential) and fastest (having the highest short-term healing rate), followed by the unaged  
 647 LDPE modified bitumen, and the unaged control bitumen heals the least and slowest.
- 648 (2) After the PAV ageing, the LDPE modified bitumen has much better healing performance  
 649 than the control bitumen and the bio-oil modified bitumen. The PAV-aged bio-oil modified  
 650 bitumen does not show any enhanced healing performance than the PAV-aged control  
 651 bitumen. The PAV-aged LDPE modified bitumen heals the most and fastest among the above  
 652 three types of PAV aged bitumen.
- 653 (3) The increased deformation recovery ability induced by LDPE in bitumen improves the  
 654 wetting rate of the cracked surfaces and leads to a higher short-term healing rate and bigger  
 655 healing. However, the LDPE in bitumen cannot accelerate the molecular diffusion to increase

656 the intrinsic healing or the long-term healing rate.

### 657 **Conflict of interest**

658 The authors declared that there is no conflict of interest.

### 659 **Acknowledgements**

660 The authors would like to acknowledge the financial support from the National Nature  
661 Science Foundation of China (Grant No. 51978229), Marie Skłodowska-Curie Individual  
662 Fellowships of EU under EU's H2020 Programme (Grant No. 789551), AIMR Seedcorn  
663 Grant from Aston University of United Kingdom (Grant No. 201901), and China Postdoctoral  
664 Science Foundation Funded Project (Grant No. 2015M571928). The authors are also grateful  
665 for the International Exchanges Grant from the Royal Society (IEC\NSFC\191252) for  
666 research collaboration.

### 667 **References**

- 668 Abo El-Naga, I., Ragab, M., 2019. Benefits of utilization the recycle polyethylene  
669 terephthalate waste plastic materials as a modifier to asphalt mixtures. *Construction and*  
670 *Building Materials* 219, 81-90.
- 671 Ahmedzade, P., Fainleib, A., Günay, T., Starostenko, O., Kovalinska, T., 2013. Effect of  
672 gamma-irradiated recycled low-density polyethylene on the high-and low-temperature  
673 properties of Bitumen. *International Journal of Polymer Science* 2013.
- 674 Ali, M.M.M., Zhao, H.Y., Li, Z.Y., Maglas, N.N.M., 2019. Concentrations of TENORMs in  
675 the petroleum industry and their environmental and health effects. *Rsc Advances* 9(67),  
676 39201-39229.
- 677 Azam, M.H., Morille, B., Bernard, J., Musy, M., Rodriguez, F., 2018. A new urban soil  
678 model for SOLENE-microclimat: Review, sensitivity analysis and validation on a car park.  
679 *Urban Climate* 24, 728-746.
- 680 Baena-González, J., Santamaria-Echart, A., Aguirre, J.L., González, S., 2020. Chemical  
681 recycling of plastic waste: Bitumen, solvents, and polystyrene from pyrolysis oil. *Waste*  
682 *Management* 118, 139-149.
- 683 Bhasin, A., Palvadi, S., Little, D.N., 2011. Influence of aging and temperature on intrinsic  
684 healing of asphalt binders. *Transportation research record* 2207(1), 70-78.
- 685 Bommavaram, R.R., Bhasin, A., Little, D.N., 2009. Determining intrinsic healing properties  
686 of asphalt binders: role of dynamic shear rheometer. *Transportation research record* 2126(1),  
687 47-54.
- 688 Cheng, D., Little, D.N., Lytton, R.L., Holste, J.C., 2002. Surface energy measurement of  
689 asphalt and its application to predicting fatigue and healing in asphalt mixtures.  
690 *Transportation Research Record* 1810(1), 44-53.
- 691 Cheng, D.X., Little, D.N., Lytton, R.L., Holste, J.C., Trb, 2002. Surface energy measurement  
692 of asphalt and its application to predicting fatigue and healing in asphalt mixtures,  
693 *Bituminous Binders 2002: Materials and Construction*. pp. 44-53.
- 694 Chew, J.-W., Poovaneshvaran, S., Hasan, M.R.M., Hamzah, M.O., Valentin, J., Sani, A.,  
695 2020. Microscopic analysis and mechanical properties of Recycled Paper Mill Sludge  
696 modified asphalt mixture using granite and limestone aggregates. *Construction and Building*  
697 *Materials* 243, 118172.
- 698 de Azevedo, A.R., Coutinho, R.A.d.S., Pereira, C.R., Cecchin, D., 2020. Characterization of  
699 solid waste of restaurant and its energy generation potential: case study of Niterói, RJ, Brazil.  
700 *Biomass Conversion and Biorefinery*, 1-10.

- 701 Farahani, H.Z., Palassi, M., Sadeghpour Galooyak, S., 2017. Thermal analysis of bitumen  
702 modified with LDPE and CR. *Petroleum Science and Technology* 35(15), 1570-1575.
- 703 Fethiza Ali, B., Soudani, K., Haddadi, S., 2020. Effect of waste plastic and crumb rubber on  
704 the thermal oxidative aging of modified bitumen. *Road Materials and Pavement Design*, 1-  
705 12.
- 706 Gallego, J., Gulisano, F., Contreras, V., Páez, A., 2021. Optimising heat and re-compaction  
707 energy in the thermomechanical treatment for the assisted healing of asphalt mixtures.  
708 *Construction and Building Materials* 292, 123431.
- 709 García-Morales, M., Partal, P., Navarro, F.J., Martínez-Boza, F., Mackley, M.R., Gallegos,  
710 C., 2004. The rheology of recycled EVA/LDPE modified bitumen. *Rheologica Acta* 43(5),  
711 482-490.
- 712 Grossegger, D., 2021. Fatigue Damage Self-Healing Analysis and the Occurrence of an  
713 Optimal Self-Healing Time in Asphalt Concrete. *Journal of Materials in Civil Engineering*  
714 33(6), 04021098.
- 715 Hariadi, D., Saleh, S.M., Yamin, R.A., Aprilia, S., 2021. Utilization of LDPE plastic waste  
716 on the quality of pyrolysis oil as an asphalt solvent alternative. *Thermal Science and*  
717 *Engineering Progress* 23, 100872.
- 718 Jalkh, R., El-Rassy, H., Chehab, G.R., Abiad, M.G., 2018. Assessment of the physico-  
719 chemical properties of waste cooking oil and spent coffee grounds oil for potential use as  
720 asphalt binder rejuvenators. *Waste and Biomass Valorization* 9(11), 2125-2132.
- 721 Karmakar, S., Kumar Roy, T., 2021. Influence of Plastic Waste on Chemical and Mechanical  
722 Properties of Modified Bitumen Used in the Bituminous Mix for Flexible Pavement. *Journal*  
723 *of Materials in Civil Engineering* 33(2), 04020440.
- 724 Kofteci, S., Nazary, M.J.C., Materials, B., 2018. Experimental study on usability of various  
725 construction wastes as fine aggregate in asphalt mixture. 185, 369-379.
- 726 Li, L., Gao, Y., Zhang, Y., 2020. Crack length based healing characterisation of bitumen at  
727 different levels of cracking damage. *Journal of Cleaner Production* 258, 120709.
- 728 Li, L., Gao, Y., Zhang, Y., 2021. Predicting healing in viscoelastic bitumen using alien strain  
729 method. *International Journal of Fatigue* 145, 106102.
- 730 Li, L., Li, W., Wang, H., Zhao, J., Wang, Z., Dong, M., Han, D., 2018a. Investigation of  
731 Prony series model related asphalt mixture properties under different confining pressures.  
732 *Construction and Building Materials* 166, 147-157.
- 733 Li, L., Li, W., Wang, Z., Dong, M., Zhang, Y., 2018b. Characterizing stress-dependent  
734 complex and relaxation moduli of dense graded asphalt mixtures. *Construction and Building*  
735 *Materials* 193, 55-63.
- 736 Li, L.L., Huang, X.M., Han, D., Dong, M.S., Zhu, D.Y., 2015. Investigation of rutting  
737 behavior of asphalt pavement in long and steep section of mountainous highway with  
738 overloading. *Construction and Building Materials* 93, 635-643.
- 739 Li, Q., Mahaffay, B., Gagnon, J., 2018. Evaluation of Asphalt Drainable Base Structural  
740 Performance for Flexible Airport Pavement Design. *Transportation Research Record*  
741 2672(23), 128-136.
- 742 Little, D., Bhasin, A., Darabi, M., 2015. Damage healing in asphalt pavements: Theory,  
743 mechanisms, measurement, and modeling, *Advances in asphalt materials*. Elsevier, pp. 205-  
744 242.
- 745 Little, D.N., Lytton, R.L., Williams, D., Kim, Y.R., Assoc Asphalt Paving Technol; Assoc  
746 Asphalt Paving, T., 1999. An analysis of the mechanism of microdamage healing based on  
747 the application of micromechanics first principles of fracture and healing.
- 748 Luo, X., 2012. Characterization of Fatigue Cracking and Healing of Asphalt Mixtures. Texas  
749 A&M University.

- 750 Luo, X., Lytton, R.L., 2016. Characterization of healing of asphalt mixtures using creep and  
751 step-loading recovery test. *Journal of Testing and Evaluation* 44(6), 2199-2210.
- 752 Lvel, J., Watson, R., Abbassi, B., Abu-Hamatteh, Z.S., 2020. Life cycle analysis of concrete  
753 and asphalt used in road pavements. *Environmental Engineering Research* 25(1), 52-61.
- 754 Lytton, R.L., 2000. Characterizing asphalt pavements for performance. *Transportation*  
755 *Research Record* 1723(1), 5-16.
- 756 Lytton, R.L., Masad, E.A., Zollinger, C., Bulut, R., Little, D.N., 2005. Measurements of  
757 surface energy and its relationship to moisture damage, Application of Surface Energy  
758 Measurements to Evaluate Moisture Susceptibility of Asphalt and Aggregates. Texas  
759 Transportation Institute, The Texas A&M University System College Station, Texas 77843-  
760 3135, p. 172.
- 761 Miglietta, F., Tsantilis, L., Baglieri, O., Santagata, E., 2021. A new approach for the  
762 evaluation of time-temperature superposition effects on the self-healing of bituminous  
763 binders. *Construction and Building Materials* 287, 122987.
- 764 Nouali, M., Derriche, Z., Ghorbel, E., Chuanqiang, L., 2020. Plastic bag waste modified  
765 bitumen a possible solution to the Algerian road pavements. *Road Materials and Pavement*  
766 *Design* 21(6), 1713-1725.
- 767 Park, S., Schapery, R., 1999. Methods of interconversion between linear viscoelastic material  
768 functions. Part I—A numerical method based on Prony series. *International journal of solids*  
769 *and structures* 36(11), 1653-1675.
- 770 Ramberg, W., Osgood, W.R., 1943. Description of stress-strain curves by three parameters.
- 771 Ramli, M.I., Pasra, M., Amiruddin, A.A., Yatmar, H., 2021. The Effect of Polypropylene  
772 (Pp) Plastic Waste on Horizontal Deformation of Concrete Asphalt, *Proceedings of the*  
773 *International Conference on Civil, Offshore and Environmental Engineering*. Springer, pp.  
774 976-982.
- 775 Romeo, E., Mantovani, L., Tribaudino, M., Montepara, A., 2018. Reuse of Stabilized  
776 Municipal Solid Waste Incinerator Fly Ash in Asphalt Mixtures. *Journal of Materials in Civil*  
777 *Engineering* 30(8).
- 778 Si, Z.S., Little, D.N., Lytton, R.L., 2002. Evaluation of fatigue healing effect of asphalt  
779 concrete by pseudostiffness. *Transportation research record* 1789(1), 73-79.
- 780 Spreadbury, C.J., McVay, M., Laux, S.J., Townsend, T.G., 2021. A field-scale evaluation of  
781 municipal solid waste incineration bottom ash as a road base material: Considerations for  
782 reuse practices. *Resources, Conservation and Recycling* 168, 105264.
- 783 Sun, B., Zhou, X., 2018. Diffusion and rheological properties of asphalt modified by bio-oil  
784 regenerant derived from waste wood. *Journal of Materials in Civil Engineering* 30(2),  
785 04017274.
- 786 Tauste-Martínez, R., Moreno-Navarro, F., Sol-Sánchez, M., Rubio-Gámez, M.C., 2021.  
787 Multiscale evaluation of the effect of recycled polymers on the long-term performance of  
788 bituminous materials. *Road Materials and Pavement Design*, 1-18.
- 789 van Oss, C.J., 2002. Use of the combined Lifshitz-van der Waals and Lewis acid-base  
790 approaches in determining the apolar and polar contributions to surface and interfacial  
791 tensions and free energies. *Journal of adhesion science and technology* 16(6), 669-677.
- 792 Wool, R., O'connor, K., 1981. A theory crack healing in polymers. *Journal of Applied*  
793 *Physics* 52(10), 5953-5963.
- 794 Xu, S., Liu, X., Tabaković, A., Lin, P., Zhang, Y., Nahar, S., Lommerts, B., Schlangen, E.,  
795 2021. The role of rejuvenators in embedded damage healing for asphalt pavement. *Materials*  
796 *& Design* 202, 109564.
- 797 Yamaç, Ö.E., Yilmaz, M., Yalçın, E., Kök, B.V., Norambuena-Contreras, J., Garcia, A.,  
798 2021. Self-healing of asphalt mastic using capsules containing waste oils. *Construction and*  
799 *Building Materials* 270, 121417.

- 800 Yan, K.Z., Li, L.L., Zheng, K.G., Ge, D.D., 2019. Research on properties of bitumen mortar  
801 containing municipal solid waste incineration fly ash. *Construction and Building Materials*  
802 218, 657-666.
- 803 Yang, Zhang, Y., Omairey, E., Cai, J., Gu, F., Bridgwater, A.V., 2018. Intermediate pyrolysis  
804 of organic fraction of municipal solid waste and rheological study of the pyrolysis oil for  
805 potential use as bio-bitumen. *Journal of Cleaner Production* 187, 390-399.
- 806 Yang, C., Xie, J., Wu, S., Amirkhanian, S., Zhou, X., Ye, Q., Yang, D., Hu, R., 2020.  
807 Investigation of physicochemical and rheological properties of SARA components separated  
808 from bitumen. *Construction and Building Materials* 235, 117437.
- 809 Zhang, Y., Gao, Y., 2019. Predicting crack growth in viscoelastic bitumen under a rotational  
810 shear fatigue load. *Road Materials and Pavement Design*, 1-20.

811

- Two waste materials were firstly used to enhance healing ability of bitumen
- Healing properties of bitumen was characterised based on crack length
- Healing rate and potential was modelled using Ramberg-Osgood Equation
- Bio-oil productively promotes healing performance of unaged bitumen
- LDPE strengthens healing performances of unaged and PAV-aged bitumen

Journal Pre-proof

To: Journal of Cleaner Production

19 June 2021

### Statement of Conflict of Interest

**Re:** submission of paper (revised version) entitled “Healing Characterisations of Waste-derived Bitumen Based on Crack Length” by Linglin Li, Yang Yang, Yangming Gao, and Yuqing Zhang to Journal of Cleaner Production.

We (all authors) wish to confirm that there are no known conflicts of interest associated with this publication, and there has been no significant financial support for this work that could have influenced its outcome.

We confirm that the manuscript has been read and approved by all named authors and that there are no other persons who satisfied the criteria for authorship but are not listed. We further confirm that the order of authors listed in the manuscript has been approved by all of us.

We confirm that we have given due consideration to the protection of intellectual property associated with this work and that there are no impediments to publication, including the timing of publication, with respect to intellectual property. In doing so, we confirm that we have followed the regulations of our institutions concerning intellectual property.

We understand that the Corresponding Author is the sole contact for the Editorial process (including Editorial Manager and direct communications with the office). He is responsible for communicating with the other authors about progress, submissions of revisions and final approval of proofs.

We confirm that we have provided a current, correct email address which is accessible by the Corresponding Author and which has been configured to accept email.

Sincerely yours,



Signed by Corresponding Author on behalf of all authors.

**Yuqing Zhang**, PhD

Senior Lecturer in Highway Engineering

Aston Institute of Materials Research (AIMR)

Engineering System & Management (ESM)

Aston University

Address: Aston Triangle, Birmingham, B4 7ET, U.K.

Tel: +44 121- 204- 3391

Email: y.zhang10@aston.ac.uk